INL/HST-23-75829-Revision-0

Loss-of-Coolant Accident Test Series Test LOC 5 Experiment Predictions

September 1979

M. E. Waterman, T. R. Yackle

Changing the World's Energy Future

INL is a U.S. Department of Energy National Laboratory operated by Battelle Energy Alliance, LLC

INL/HST-23-75829-Revision-0

Loss-of-Coolant Accident Test Series Test LOC 5 Experiment Predictions

M. E. Waterman, T. R. Yackle

September 1979

Idaho National Laboratory
Idaho Falls, Idaho 83415

http://www.inl.gov

Prepared for the
U.S. Department of Energy
Under DOE Idaho Operations Office
Contract DE-AC07-76IDO1570

TFBP-TR-332
for U.S. Nuclear Regulatory Commission

LOSS-OF-COOLANT ACCIDENT TEST SERIES
TEST LOC 5
EXPERIMENT PREDICTIONS

M.E. WATERMAN T.R. YACKLE

September 1979

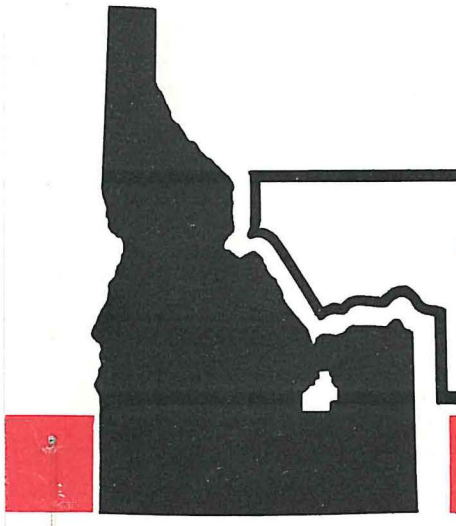

EG&G Idaho, Inc.

IDAHO NATIONAL ENGINEERING LABORATORY

DEPARTMENT OF ENERGY

IDAHO OPERATIONS OFFICE UNDER CONTRACT DE-AC07-76IDO1570

TFBP-TR-332
September 1979

PBF-LOCA TEST SERIES

TEST LOC-5

EXPERIMENT PREDICTIONS

M. E. Waterman
T. R. Yackle

Approved:

R. K. McCardell

R. K. McCardell, Manager
PBF Experiment Specification and Analysis Branch

R. K. McCardell for

P. E. MacDonald, Manager
LWR Fuel Research Division

EG&G Idaho, Inc.

FORM EG&G-398
(Rev 12-78)

INTERIM REPORT

Accession No. _____

Report No. TFBP-TR-332

Contract Program or Project Title: Thermal Fuels Behavior Program

Subject of this Document: Loss-of-Coolant Accident Test Series Test LOC-5 Experiment Prediction Document

Type of Document: EPD

Author(s): M. E. Waterman, T. R. Yackle

Date of Document: September 1979

Responsible NRC Individual and NRC Office or Division:

This document was prepared primarily for preliminary or internal use. It has not received full review and approval. Since there may be substantive changes, this document should not be considered final.

EG&G Idaho, Inc.
Idaho Falls, Idaho 83401

Prepared for the
U.S. Nuclear Regulatory Commission
and the U.S. Department of Energy
Idaho Operations Office
Under contract No. DE-AC07-76ID001570
NRC FIN No. A6041

INTERIM REPORT

The RELAP4 and FRAP-T model and code updates utilized for the LOC test predictions contained in this report have been reviewed by the EG&G PBF Pretest Prediction Consistency Committee.

D. R. Coleman
Code Assessment and Application
Program Representative

D. W. Croucher
Thermal Fuels Behavior Program Representative

J. L. Steiner
Semiscale Program Representative

G. W. Johnsen
Code Development and Application Program Representative

W. H. Grush
LOFT Program Representative

SUMMARY

The Loss of Coolant Accident (LOCA) Test Series being conducted in the Power Burst Facility (PBF) at the Idaho National Engineering Laboratory has been designed to provide data for the development and the assessment of fuel behavior computer codes used to predict the response of a pressurized light water reactor (PWR) during a hypothetical break in the cold-leg inlet or hot-leg outlet. This report presents the experiment predictions for the four-rod LOCA test, LOC-5.

Test LOC-5 will be performed using Saxton design fuel rods. Two of the fuel rods are unirradiated and two rods are irradiated to about 16000 to 17000 MWd/t. One of each set of the irradiated and the unirradiated rods will be backfilled with helium to a pressure typical of beginning-of-life PWR fuel rods, while the other rods will be backfilled to a pressure typical of fuel rods at the end-of-operational life. Each rod will be surrounded by an individual coolant flow shroud.

The test sequence will consist of a loop heatup phase, a steady state phase, a blowdown phase, a reflood phase, and a quench phase. The purpose of the steady state phase is to perform the fuel rod power calibration and to precondition the fuel. In the blowdown and reflood phase, the fuel rods will be subjected to a system depressurization typical of a double-ended cold-leg break LOCA with reflood.

An analysis was performed to predict the test fuel rod and system behavior during a typical LOC test. Reactor physics calculations were performed with the RAFFLE code to determine the relationship between test fuel rod powers and the PBF reactor power during both the steady state operation and during the blowdown. Calculation of the system thermal-hydraulic response during blowdown, made with the RELAP4 computer code, provided the coolant and heat transfer boundary conditions for the fuel behavior calculations. Cladding and fuel rod dimensions for the rods previously irradiated in the Saxton reactor

were determined with the FRAP-S code. Finally, the rod thermal and mechanical behavior during the blowdown transient were determined with the FRAP-T5 code.

Based on the LOC-5 analysis described herein, isolating the PBF primary loop from the test train and opening both cold-leg valves will result in a system depressurization typical of a PWR double-ended cold-leg break LOCA. The system will depressurize within 35 seconds. During the initial subcooled depressurization, the system cold-leg pressure will decrease from 15.51 MPa to 10.5 MPa in 100 ms as the subcooled liquid discharges from the blowdown system into the blowdown tank. Following the subcooled depressurization, the liquid in the cold-leg will begin flashing and two-phase choked flow conditions will be established in the cold-leg Henry nozzles. The saturated depressurization will then be limited by flow choking at the nozzles until blowdown is complete. The coolant in the hot-leg and test train upper plenum regions will remain at a higher pressure than the test train lower plenum throughout the blowdown. The upper-to-lower pressure differential will close the check valves located at the top of each fuel rod flow shroud and prevent the flow of coolant from the upper plenum into the flow shrouds. The coolant within each flow shroud will exit the bottom of the shroud into the lower plenum during blowdown. Voiding of the coolant in each flow shroud will result in propagation of fuel rod critical heat flux up the fuel rod within 0.3 s, starting on the lower region of the fuel rod. Following CHF, the modes of fuel rod heat transfer will be: (1) a brief period of transition film boiling, (2) stable film boiling, and (3) forced and natural convection to steam in combination with radiation to flow shroud and steam.

The prior irradiation of two of the fuel rods is predicted to have strengthened the cladding, densified the fuel, and reduced the cladding diameter. The effect of increased cladding strength is predicted to be more significant for the low pressure irradiated fuel rod than for the high pressure irradiated fuel rod and is predicted to effect fuel rod behavior only during the first 2 s of the blowdown.

The increased cladding strength is predicted to retard the initial amount of cladding collapse that is predicted to occur in the low pressure irradiated rod. The densification of the fuel in the irradiated rods is predicted to result in larger fuel-to-cladding gap sizes and higher internal rod pressures than in the unirradiated rods. The larger gap sizes will result in higher fuel stored energies at the onset of the transient and subsequently higher peak cladding temperatures at the thermocouple locations later in the transient. The densification of the fuel in the irradiated rods is also predicted to result in higher initial internal rod pressures due to higher fuel and internal rod gas temperatures and result in a faster rate of cladding ballooning for both irradiated rods as compared to the unirradiated rods. The cladding diameter of the irradiated rods is predicted to have been reduced (while in the Saxton reactor) due to creep. The effect on the gap heat transfer coefficient due to the reduced diameter in the previously irradiated rods is predicted to be offset by the reduction in fuel pellet diameter due to fuel densification. The reduction in cladding diameter will also result in some cladding strengthening due to cold working; however, the effect of the increased cladding strength is predicted to anneal out at the elevated cladding surface temperatures that are predicted to occur during the transient.

The cladding temperatures are expected to increase to approximately 1450 K, then decrease and stabilize. The two test rods with the low pressures are predicted to reach temperatures of approximately 1400 K at the time of burst (9-10 s) and strains at failure of approximately 26 to 30%. The high pressure rods are expected to fail earlier (4 s) at lower temperatures of about 1200 K and at strains of 15 to 22%.

Cladding ballooning within the lower portion of the high power region of each rod is predicted during blowdown and will depend upon the cladding history, the local time-to-CHF, and the difference between rod internal pressure and system pressure during blowdown. The pressure inside the low pressure rods will not exceed system

pressure until the cladding temperatures have reached the $\alpha + \beta$ phase and; therefore, the cladding of these rods is not predicted to begin ballooning until the cladding temperatures are in the high $\alpha + \beta$ phase. Cladding failure is not predicted until the cladding temperatures reach the β phase. In contrast the higher pressure rods are predicted to deform and fail while the cladding temperatures are still in the $\alpha + \beta$ phase.

The data of Test LOC-5 will be valuable in assessing the analytical models used to make these predictions. These data, combined with the data from LOCA single-rod tests, will be used to better understand fuel rod behavior during a simulated double-ended cold-leg break LOCA.

CONTENTS

FIGURES

TABLES

1. INTRODUCTION

The Loss of Coolant Accident (LOCA) Test Series[1] is part of the Department of Energy Fuel Behavior Program[2] sponsored by the Nuclear Regulatory Commission and is directed towards providing a detailed understanding of the response of nuclear fuel rods to off-normal accident conditions. This program is one of several programs being conducted by EG&G Idaho, Inc. in the Power Burst Facility (PBF) that will provide data for development and assessment of fuel behavior computer models used to predict the response of LWR fuel under hypothetical accident conditions.

The LOCA tests simulate accidents resulting from a break in the cold-leg inlet or hot-leg outlet of a pressurized water reactor (PWR) core. During a LOCA, the coolant conditions are characterized by a rapid core depressurization and drastic changes in both coolant mass flow and quality. Depending upon the break size and location in the cold- or hot-leg, system depressurization will be completed within approximately 35 s. Cooling of the fuel rods will degrade during the accident and the fuel rod cladding will heat up and may balloon and rupture.

The purpose of this document is to present the experiment predictions for Test LOC-5. The test will be performed using four separately shrouded fuel rods of PWR 15x15 design. Two rods have been previously irradiated and two rods are unirradiated. One unirradiated and one irradiated rod will be backfilled with helium to a pressure typical of beginning-of-life PWR fuel rods (2.41 MPa), and the other two rods will be backfilled to a pressure typical of fuel rods at the end-of-operational life (4.83 MPa).

The behavior of PWR fuel rods with different initial internal pressures and irradiation histories during a double-ended cold-leg break LOCA, with the cladding in the β phase temperature range, will be investigated during the LOC-5 test.

The test will be performed in five separate phases; loop heatup, preconditioning operation, blowdown, reflood, and quench. The primary loop coolant conditions will be increased to the desired pressure and temperature. The test rods will be power cycled during the preconditioning phase and then operated at steady state for approximately 1-1/2 hours to build up the desired fission product inventory. The blowdown will follow with the system conditions similar to those expected in a PWR during a postulated double-ended cold-leg break. Reflood will be initiated and the transient will be terminated following the system reflood with quench and long-term cooling to remove decay heat.

Section 2 of this document briefly describes the fuel rods, test train, and LOCA blowdown system. Section 3 presents the experiment conduct. Section 4 discusses the experiment predictions and these predictions are summarized in Section 5. Appendix A presents the FRAP computer models used in the analysis.

2. EXPERIMENT DESIGN

This section provides a summary description of the fuel rods, test train, and LOCA blowdown system hardware for Test LOC-5. Detailed hardware and instrumentation descriptions are provided in the Experiment Specification Document[3].

2.1 Fuel Rods and Shrouds

The fuel rods consist of two Saxton rods previously irradiated to about 16000 to 17000 MWd/t in the Saxton reactor, and two unirradiated Saxton rods. The two irradiated rods are designated 605-6 and 605-8, while the two unirradiated rods are designated as 605-5 and 605-7. The dimensional characteristics of each rod are typical of PWR fuel rods except for total length and plenum volume. The as-fabricated nominal design characteristics of these fuel rods are given in Table I. Rods 605-5 and 605-6 are prepressurized to 2.41 MPa helium, typical of a PWR rod beginning-of-life pressure, and Rods 605-7 and 605-8 are prepressurized to 4.83 MPa helium, typical of a PWR rod end-of-life pressure. A cross section of the fuel rod orientation and instrumentation is shown in Figure 1.

2.2 Test Train

The LOC-5 test train positions and supports the four test fuel rods in the in-pile tube (IPT) as shown in Figures 1 and 2. Major test train components are the fuel rod support plates, the IPT flow tube, the flux shaper, particle screens and catch basket, filler pieces and the reflood line.

The fuel rod support plates position each rod within the active core region. The top of each rod is fixed to the upper support plate. The lower support plate is not fixed to the fuel rods so that each rod is allowed to expand axially downward.

TABLE I

TEST LOC-5 FUEL ROD NOMINAL DIMENSIONS

Cladding material - zircaloy-4

Cladding outside diameter - 9.93 mm

Cladding inside diameter - 8.75 mm

Cladding wall thickness - 0.59 mm

Diametral gap - 0.216 mm (unirradiated)

Pellet diameter - 8.534 $\pm$ 0.013 mm (Rods 605-5, 605-7),
8.484 $\pm$ 0.013 mm (Rod 605-6, 605-8)

Pellet length - 15.24 $\pm$ 0.25 mm

Pellet dish depth - 0.34 mm, spherical radius - 16.08 mm

Pellet centerhole[a] - 1.88 $\pm$ 0.05 mm (unirradiated)

Fuel length - 889 mm

Top insulating pellet length - 15.24 $\pm$ 0.25 mm

Bottom insulating pellet length - 6.35 $\pm$ 0.25 mm (unirradiated rods)

Plenum volume - 2.917 cm^3 (included plenum pressure transducer and sensor line volumes)

a. Drilled for centerline thermocouple placement.

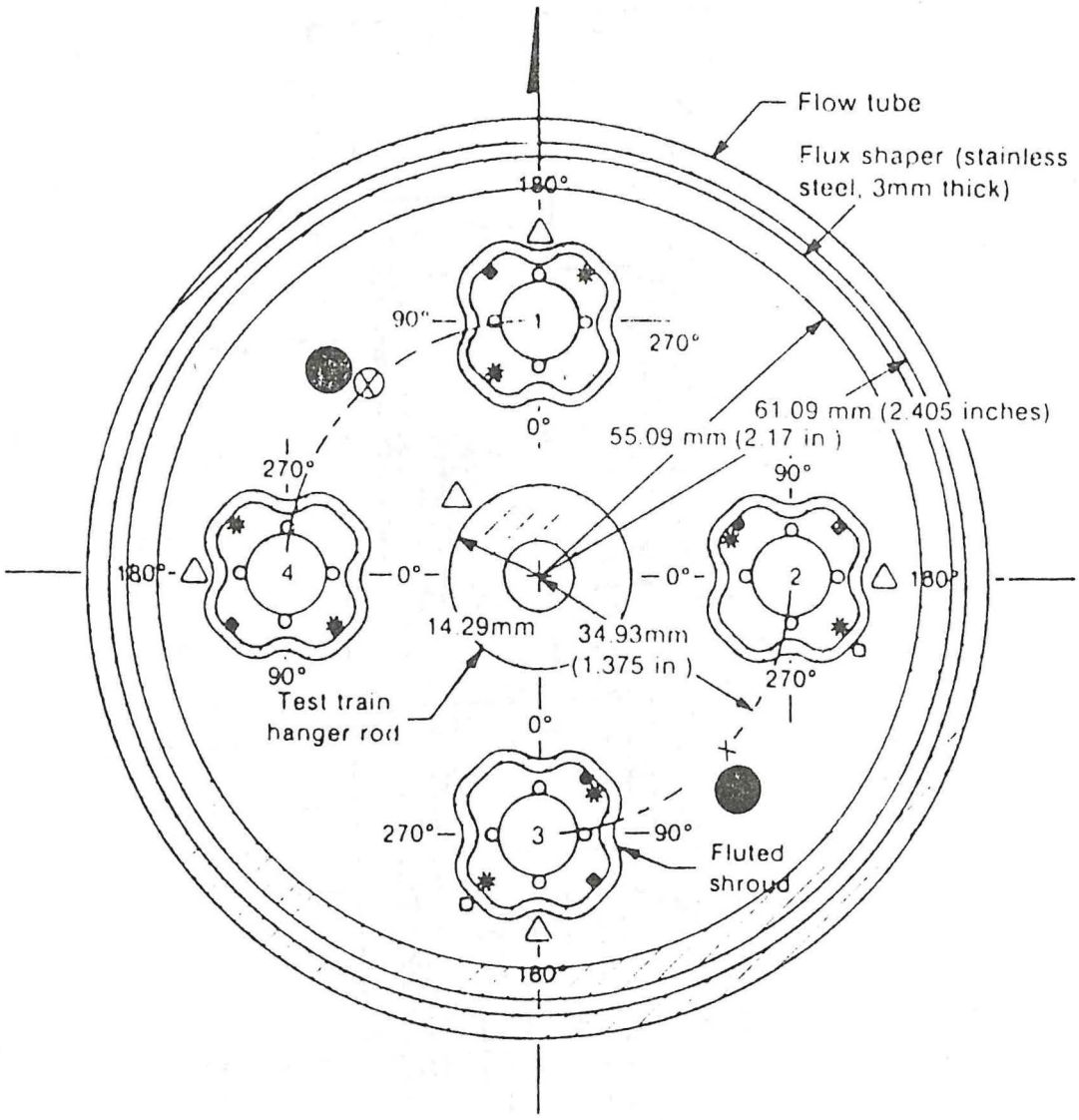

Rod locations	Rod No	Internal pressure
1	605-5	(2.41 MPa)
2	605-6	(2.41 MPa)
3	605-7	(4.83 MPa)
4	605-8	(4.83 MPa)

Rod to rod pitch - 49.39 mm

- o Cladding thermocouples
- x Self powered neutron detectors
- ⊗ Self powered gamma detectors
- ● Zircaloy-4 support tube - 10.9 mm outer diameter
- △ Flux wires
- ● Inside shroud coolant thermocouples
- □ Outside shroud surface thermocouples
- ✱ Differential thermocouple
- ■ Inlet/outlet thermocouple

Fig. 1 Test LOC-5 fuel train orientation. INEL-A-10 340

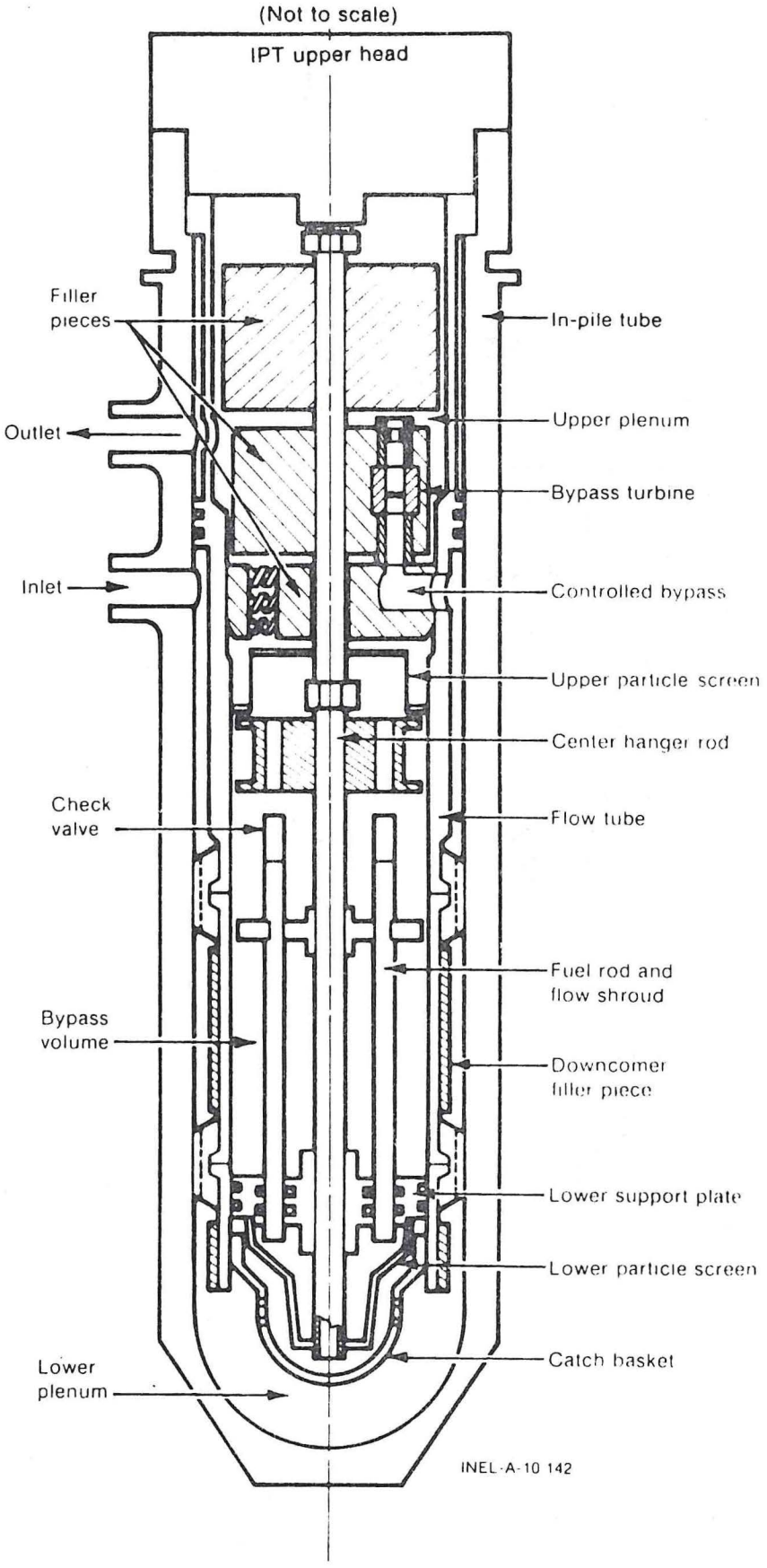

Fig. 2 Test LOC-5 test train illustration.

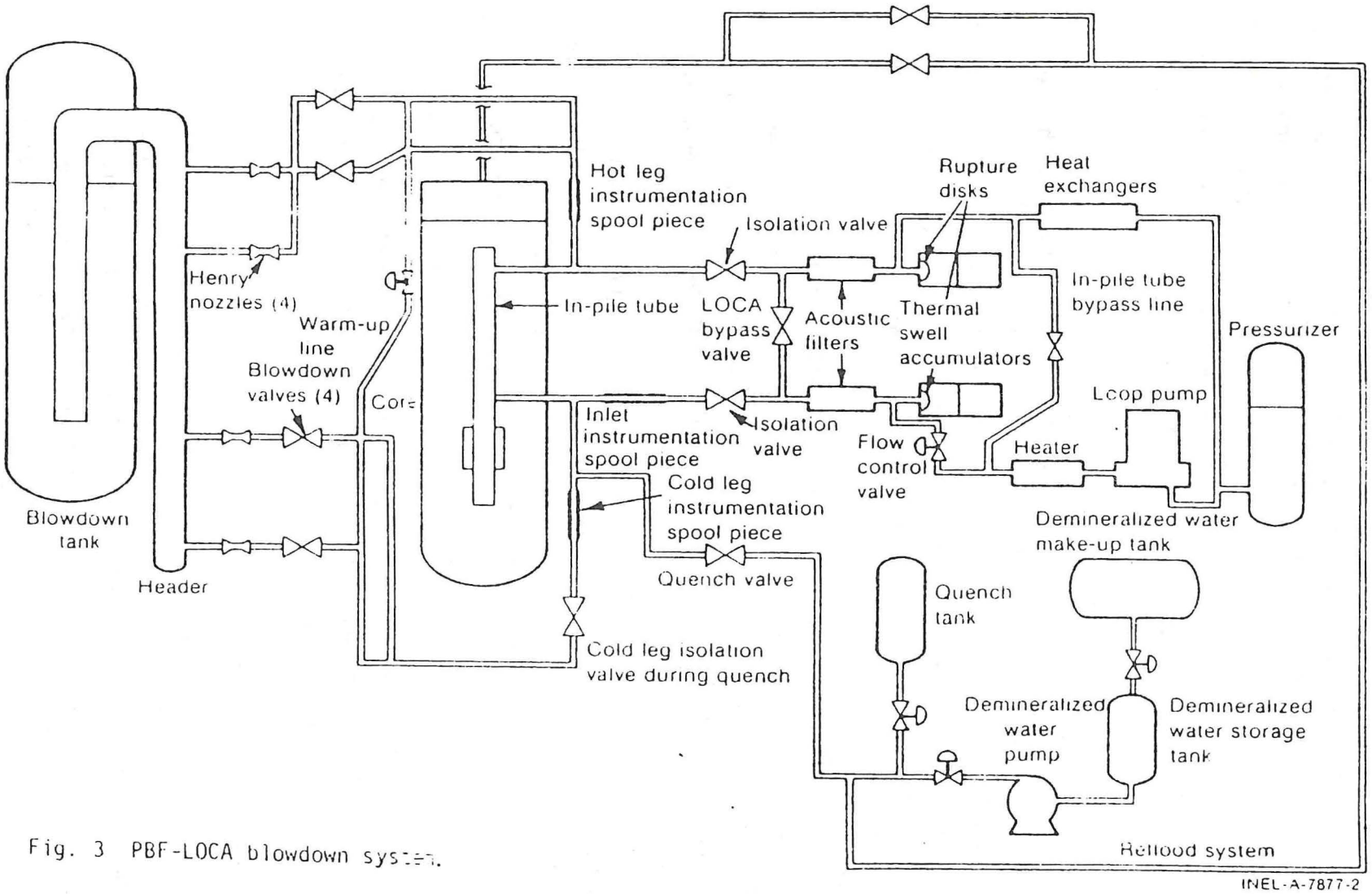

Fig. 3 PBF-LOCA blowdown system.

The IPT flow tube directs the coolant from the IPT inlet down to the lower plenum and up into the fuel rod flow shrouds. The IPT flow tube is fabricated in three sections, two of stainless steel and one of zircaloy. The zircaloy section is positioned in the central core region. A stainless steel flux shaper is located within the zircaloy section to flatten the axial power profile in the central test train region.

All coolant that passes the fuel rods is channeled through lower and upper particle screens, with the 5 mil screen mesh sizes equivalent to the mesh sizes of the screens in the blowdown measurement spools. A catch basket is located below the lower particle screen to catch any fuel and protect the IPT.

Filler pieces are located in the IPT exit volume, the upper plenum, and the downcomer region to minimize the volume of water in the test train. Each filler piece is sized to allow the maximum water volume reduction while still providing sufficient coolant flow area.

A bypass path between the IPT inlet and the upper plenum is contained in the upper plenum filler piece. The bypass provides a low resistance flow path between the upper plenum and inlet during blowdown and includes the capability of being orificed to reduce the flow area.

The capability to directly inject reflood water into the lower plenum is available through the zircaloy hanger rod tube and will be used during the LOC-5 test.

2.3 LOCA Blowdown System

The PBF-LOCA blowdown loop is illustrated in Figure 3. The blowdown system provides the means to isolate the IPT from the existing loop during blowdown and directs the coolant into the blowdown tank. Blowdown is initiated by quick opening and closing

of the valves. Four Henry nozzles, two in the cold leg and two in the hot leg, provide the break plane for the desired break flow rate and depressurization rate.

A small line connects the hot and cold blowdown piping legs with a controllable valve. This line provides a small flow rate to keep the hot and cold legs at a constant temperature prior to blowdown. The valve and line also provide additional means of controlling the coolant mass flow through the fuel assembly.

The blowdown header and tank collect and contain the coolant ejected from the IPT and piping during blowdown, reflood, quench, and postblowdown cooling. It will also contain any fission products carried from the fuel rods by the coolant.

IPT reflood is accomplished by the opening of the reflood valves (shown at the top of Figure 3) thereby allowing reflood coolant to enter the lower plenum of the IPT through the hanger rod.

Test termination by quench is accomplished by opening the quench valve (and closing the cold leg blowdown valves) to permit coolant from the quench tank to enter the IPT. The quench tank is pressurized by a nitrogen gas system and heated to 366 K. After the quench tank has emptied (in about 60 s) coolant is pumped from the storage tank through the hot water tank for up to a four hour period. If needed, additional longer term cooling can be accomplished by reconnecting the IPT to the primary coolant loop by opening the isolation valves and closing the bypass blowdown valves.

The sequencing of the valve operation during blowdown is controlled by a time-sequential programmer in the Programming and Monitoring Systems (P&MS). Signals for cladding temperature and time are input to the P&MS.

3. EXPERIMENT CONDUCT

Details of the experiment procedure for Test LOC-5 are summarized in this section. The test operating sequence is shown in Figure 4. A detailed description of the test conduct is provided in the LOC-5 Experiment Operating Specification[4].

3.1 Heatup Phase

System coolant conditions will be established at 15.5 MPa and 590 K at the lower plenum during the heatup phase. Instrument status checks will be completed and the loop and test train flow meters will be intercalibrated.

3.2 Power Calibration Phase

Individual fuel rod powers will be determined by an energy balance method during the power calibration phase. To perform the calibration, the reactor power will be increased to a known level, the system allowed to stabilize, and the test rod power and self-powered neutron detector (SPND) outputs recorded. This procedure will be repeated at a number of power levels up to a maximum reactor power of approximately 26 MW.

3.3 Preconditioning Phase

The four fuel rods will be preconditioned with three power cycles, each reaching a peak rod power of 52.0 kW/m, to promote fuel pellet cracking and restructuring and to allow pellet-cladding mechanical interaction to stabilize. The power ramp rate of each cycle will be a maximum of 2 kW/m-min with the power maintained at the peak of each cycle for approximately 10 minutes.

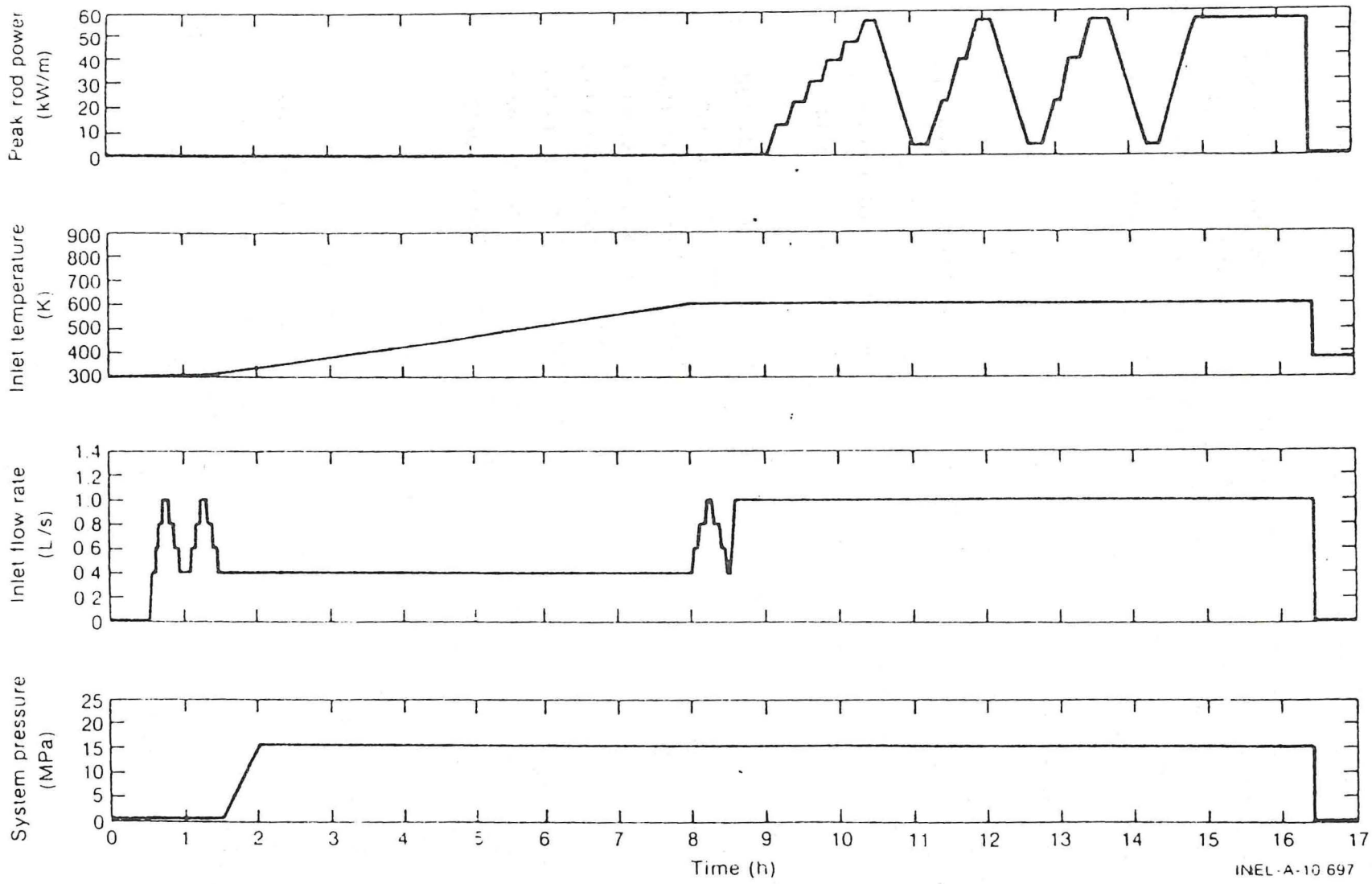

Fig. 4 Test LOC-5 operating sequence.

3.4 Decay Heat Buildup Phase

After completion of the preconditioning phase, the peak fuel rod power will be increased to 52.0 kW/m at a rate of 2 kW/m-min. This power level will be maintained for 1-1/2 hours, the length of time necessary to build up approximately 78% of the maximum possible decay heat in the rods.

3.5 Blowdown Phase

The specific steps of the blowdown and reflood phase are provided in Table II. This particular sequence was selected to achieve critical heat flux shortly after initiating blowdown and to provide a steam environment for the test fuel rods during blowdown and reflood.

The cladding temperatures at the peak power region are predicted to rise rapidly during blowdown and to stabilize within the β-phase. A goal of the LOC-5 test is to maintain these temperatures within the β phase (> 1350 K) out to 50 s. Initial pretest analyses demonstrated that radiation heat transfer from the fuel rods to the individual flow shrouds was excessive, and that cladding temperatures would fall below the desired temperature range. Therefore, the test operating sequence was modified to have the PBF core operated at low power levels during blowdown to maintain a small power within each test rod and keep cladding temperatures within the β-phase region.

The reactor power will be controlled with the transient rods during blowdown. The transient rods will be preprogrammed to decrease the rod power from the initial steady state power to a low power and simultaneously compensate for reactivity changes associated with voiding of the in-pile tube. The position history for the transient rods was determined by pretest analyses.

TABLE II

PROGRAMMING AND MONITORING SYSTEM CONTROLLED EVENT SEQUENCE

Step	Estimated Time REDCOR Signal Is Initiated (s)[a]	Time Event Is Initiated (s)	Loop Bypass Valve[b]	Isolation Valve[c]	Hot Leg Blowdown Valves[d]	Cold Leg Blowdown Valves[e]	Quench Water Valve[f]	Warm-up Line Valve[g]	Cold Leg Shutoff Valve[h]	Comments
Initial	--	--	X[i]	0	X	X	X	0	0	Cladding scram set points turned off.
1	--	-20.0	X	0	X	X	X	X	0	Operator closes warmup line and verifies test rod coolant flow to 1.0 l/s per shroud. Action is verified by TFBP Project Engineer before initiation of the transient.
2	-2.0	-2.0	X	0	X	X	X	X	0	REDCOR initiates function generator routine.
3	-0.07	0.00	0	X	X	X	X	X	0	Isolate loop and open bypass valve.
4	-0.03	0.10	0	X	X	0	X	X	0	Open cold leg valves.
5	0.00	2.50	0	X	X	0	X	X	0	Maintain 100% of reactor power.
6	2.50	2.80	0	X	X	0	X	X	0	Linearly reduce reactor power to 25.50% in 0.3 s.

TABLE II (continued)

Step	Estimated Time REDCOR Signal Is Initiated (s)[a]	Time Event Is Initiated 's)	Loop Bypass Valve[b]	Isolation Valve[c]	Hot Leg Blowdown Valves[e]	Cold Leg Blowdown Valves	Quench Water Valve[f]	Warm-up Line Valve[g]	Cold Leg Shutoff Valve[h]	Comments
7	2.80	2.80	0	X	X	0	X	X	0	Linearly reduce reactor power to 12.75% in 2.2 s.
8	5.00	5.00	0	X	X	0	X	X	0	Linearly reduce reactor power to 7.95% in 5.0 s.
9	10.00	10.00	0	X	X	0	X	X	0	Linearly reduce reactor power to 6.80% in 2.0 s.
10	12.00	12.00	0	X	X	0	X	X	0	Linearly reduce reactor power to 6.37% in 8.0 s.
11	20.00	20.00	0	X	X	0	X	X	0	Maintain reactor power at 6.37%.
12	50.00	50.10	0	X	X	0	X	X	0	Scram reactor.
13	70.00	70.00	0	X	X	X	X	X	0	Reflood cycle.
14	240	240	0	X	0	X	0	X	X	Quench

'a) Times are estimated for REDCOR signal. Final signal specification will be determined by the PBF Operations Branch.
(b) VALVbPOSbbLM1107PT
(c) VALVbPOSbbLM1105PT and VALVbPOSbbLM1106PT
(d) VALVbPOSbbLM1101PT and VALVbPOSbbLM1102PT
(e) VALVbPOSbbLMLRC1PT and VALVBPOSbbLMLRC2PT
(f) VALVbPOSbbLM1108PT
(g) VALVbPOSbbLM1116PT
(h) VALVbPOSbbLM1118PT
(i) X indicates closed, 0 indicates open.

3.6 Reflood Phase

The reflood phase of the test will begin 70 s after initiation of blowdown. The controlled reflood is performed by injecting coolant through the reflood system into the IPT head, down the center of the hanger rod into the plenum beneath the lower particle screen. The sequence of events involves: (a) filling the lower plenum to the bottom of the active core within 5 s and maintaining this level prior to reflood of the fuel rods, and (b) providing constant core reflood rate to the flow shrouds. The system pressure at the time of reflood initiation will be approximately 0.45 MPa and the reflood coolant temperature will be 311 K at the entrance to the IPT upper head.

3.7 Quench and Cooldown Phase

After 240 s, posttest quench cooling water, heated to 366 K, will be injected into the coolant system at 4 l/s for 60 s.

After quench, cooling water will be pumped from the coolant storage tanks for 60 s. Beyond this time, the cooling water flow rate will be reduced from 4 l/s to 0.4 l/s. Longer term cooling will be provided, if necessary, by the primary loop after reconnection to the IPT.

4. EXPERIMENT PREDICTIONS

The experiment predictions for Test LOC-5 are presented in this section. The predictions are based on analyses performed in the following areas:

(1) reactor physics
(2) system thermal-hydraulic response
(3) fuel rod steady state and transient response.

The reactor physics, system thermal hydraulic response, and the fuel rod steady state response have been examined and are considered the same as the analyses performed in the Test LOC-3[5]. Therefore, the fuel rod behavior analysis during the transient phase of the test will be the only area discussed in this report.

4.1 Fuel Rod Behavior Analysis

FRAP-T5[a] predictions of the behavior of the LOC-5 fuel rods during the transient phase of LOC-5 test are presented in this section.

The fuel rod behavior calculations were performed using an initial peak fuel rod linear power of 52.0 kW/m, and system thermal-hydraulic conditions of 15.51 MPa coolant inlet pressure, 590 K coolant inlet temperature, and 1.0 l/s coolant inlet flow rate. The transient sequence consisted of loop isolation at time zero followed by initiation of system depressurization at 0.1 s. The loop geometry was unchanged for the subsequent 50 s. The power history shown in Figure 5 was developed from RELAP4[b], FRAP-T5[6], and reactor physics calculations.

---

a. FRAP-T5, Idaho National Engineering Laboratory, Configuration Control Number H003784B.
b. RELAP4/MOD6/UPDATE4, Idaho National Engineering Laboratory, Configuration Control Number H00598IB.

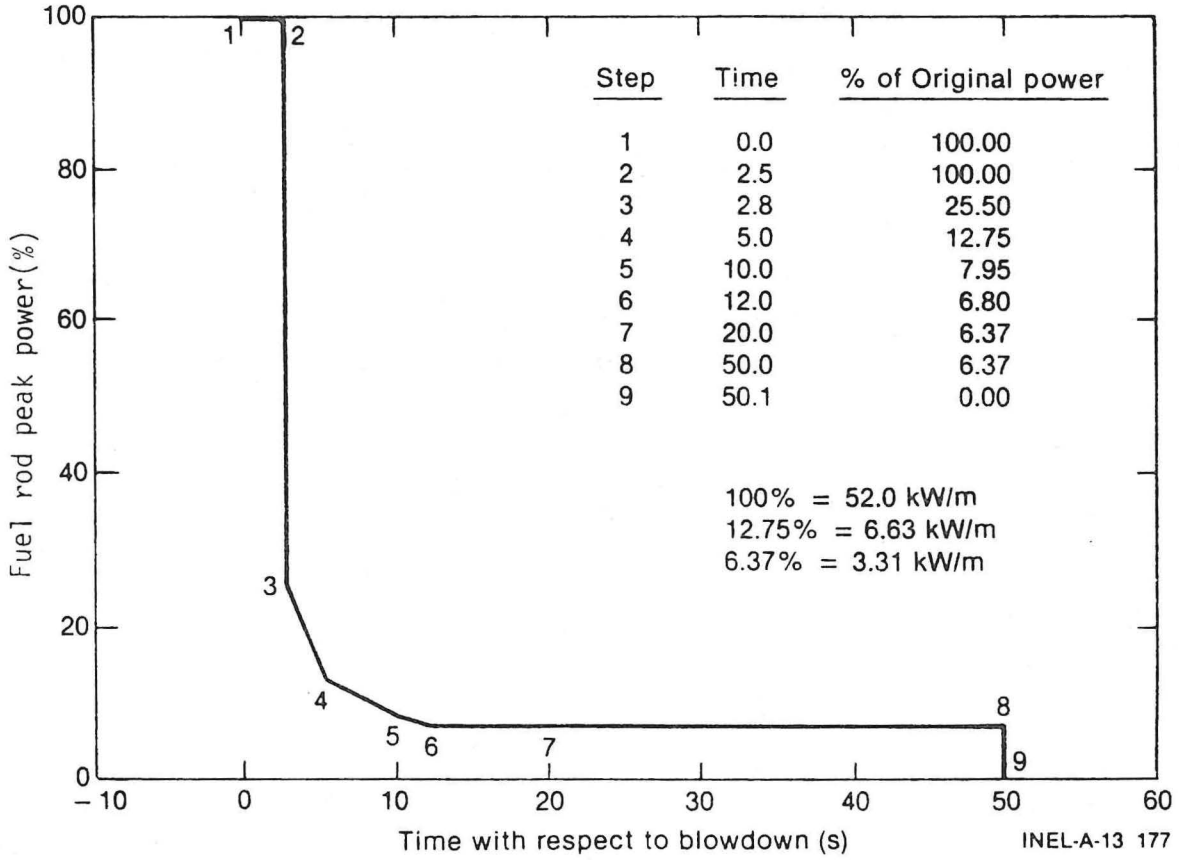

Fig. 5 Fuel rod peak power variation with time during the transient.

The LOC-3 RELAP4 calculations were used for the LOC-5 pretest predictions. However, the thermal-hydraulic data input for the LOC-5 FRAP-T5 pretest predictions were changed to account for the axial variation of time-to-CHF. This was done by shifting the RELAP-generated uniform time-to-CHF thermal-hydraulic values forward or back with respect to time according to the observed LOC-3 times-to-CHF.[7] As a consequence, the test predictions should more accurately predict fuel rod behavior in the LOC-5 test. The axial distribution of time-to-CHF used for the LOC-5 pretest predictions is shown in Figure 6.

4.1.1 Fuel Rod Temperature Response. A discussion of the predicted LOC-5 fuel rod temperature response at the thermocouple locations and at the location of the cladding peak temerature is provided in this subsection.

4.1.1.1 Temperature response at the thermocouple locations. The cladding surface temperatures at the cladding and fuel centerline thermocouple locations and the fuel centerline temperature at the fuel centerline thermocouple location are shown in Figures 7 through 10 for Rods 605-5, 605-6, 605-7 and 605-8, respectively.

The cladding temperatures at 0.580, 0.630, and 0.680 m, and the fuel centerline temperature at 0.580 m are presented in Table III for the LOC-5 fuel rods (at the time of maximum cladding temperature of the 0.580 m location). The difference in the cladding surface temperatures in Table III between the 0.580 m and 0.680 m locations ($\sim$200 K for every rod) is due to the axial power distribution and the estimated time of CHF at each elevation. The local rod power was higher at 0.580 m than at 0.680 m, and subsequently resulted in a greater amount of fuel stored energy at 0.580 m than at 0.680 m at the beginning of the transient. Thus, initially higher fuel temperatures, and consequently higher cladding temperatures, were predicted at 0.580 m than at 0.680 m. The time-to-CHF at the 0.580 m location was estimated to be 2.25 s; whereas, the time-to-CHF at the 0.680 m location was estimated to be 3.75 s, as shown in Figure 6. During the 1.5 s interval between these two times, the cladding surface

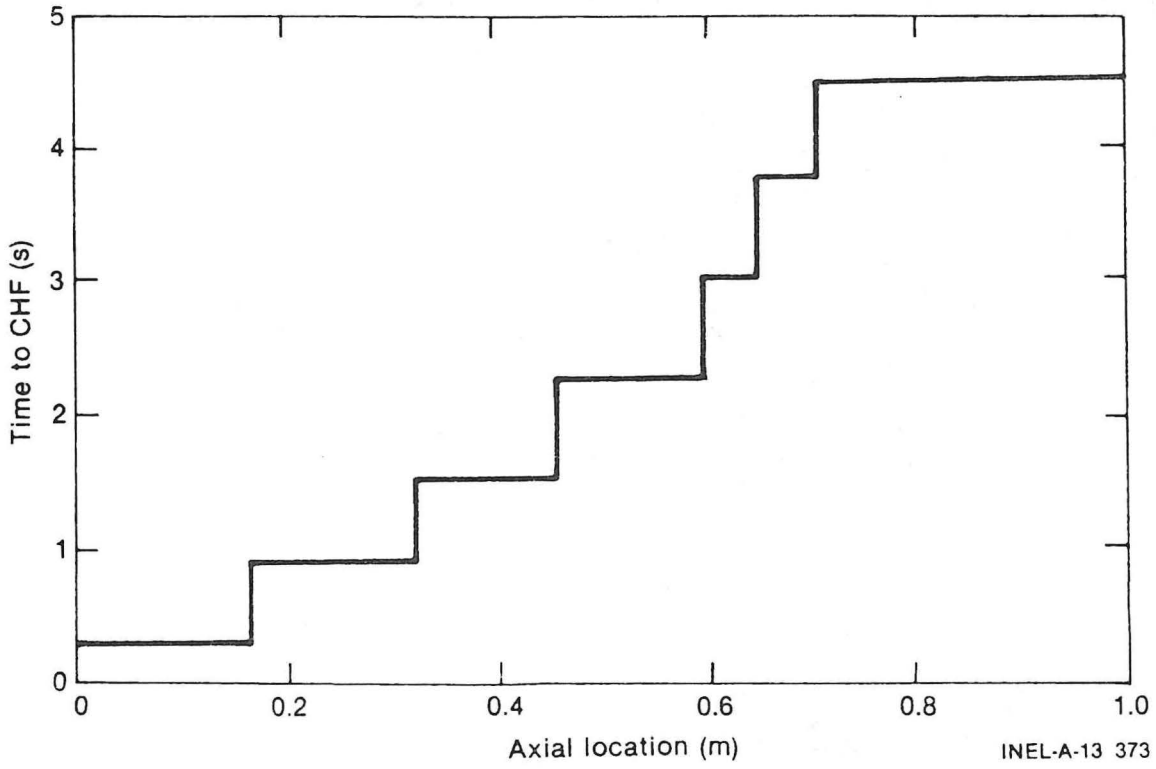

Fig. 6 The time-to-CHF as a function of axial location.

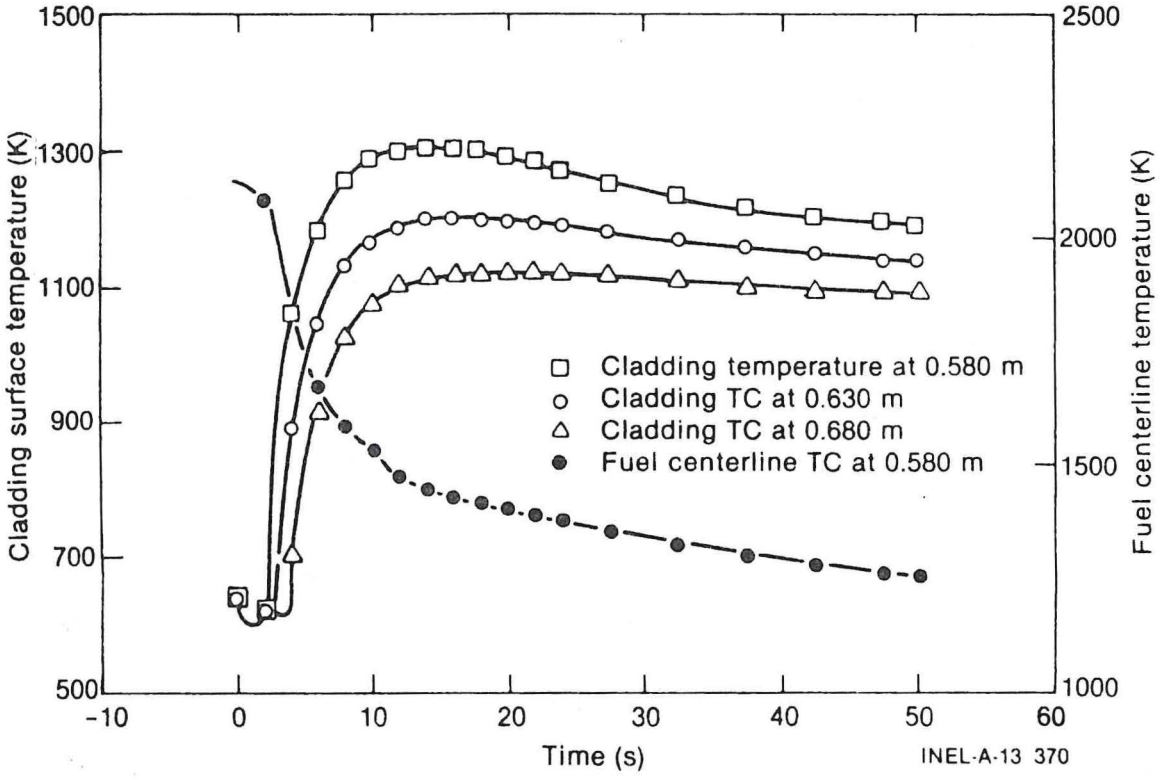

Fig. 7 Rod 605-5 fuel centerline and cladding surface temperatures at the thermocouple locations.

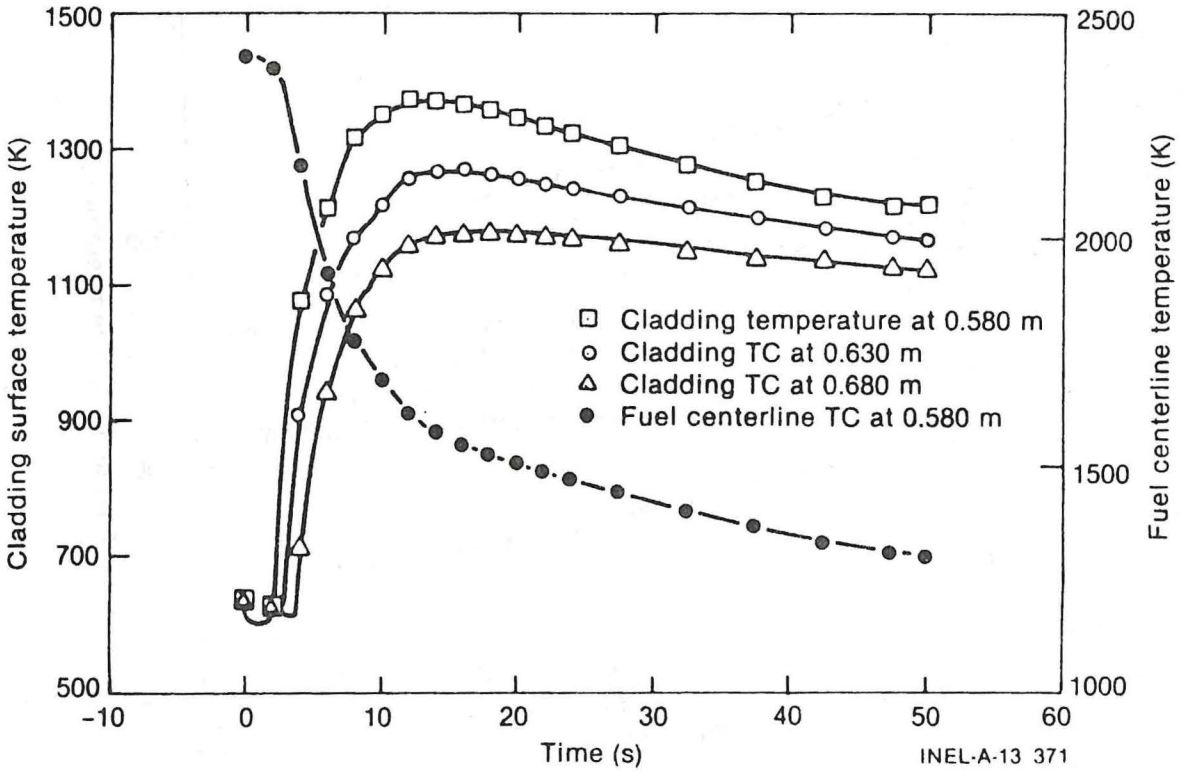

Fig. 8 Rod 605-6 fuel centerline and cladding surface temperatures at the thermocouple locations

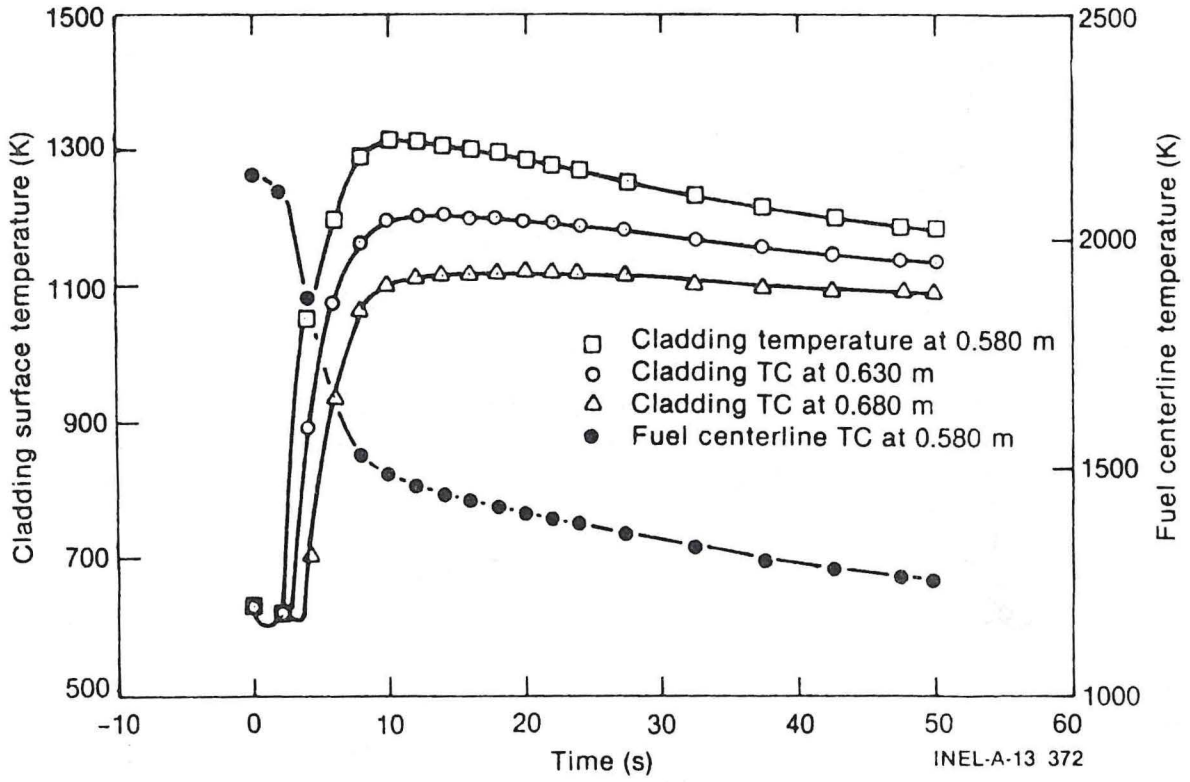

Fig. 9 Rod 605-7 fuel centerline and cladding surface temperatures at the thermocouple locations.

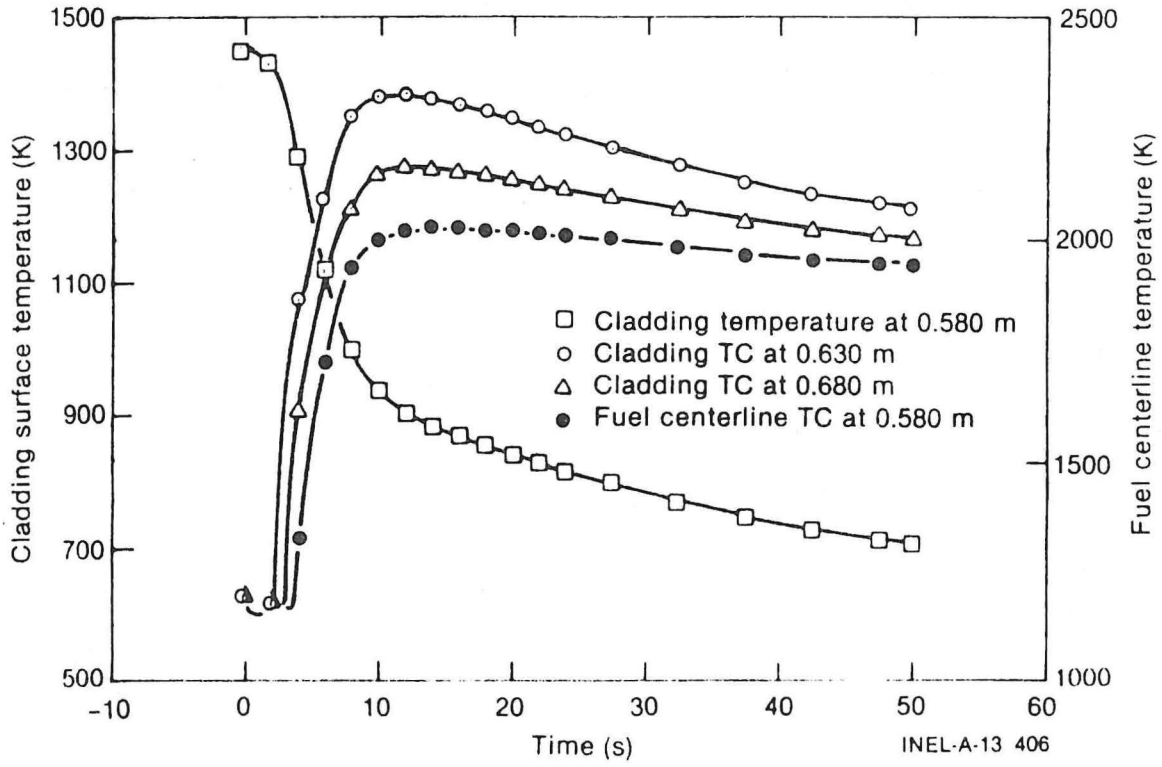

Fig. 10 Rod 605-8 fuel centerline and cladding surface temperatures at the thermocouple locations.

TABLE III

FUEL ROD TEMPERATURES AT THE THERMOCOUPLE LOCATIONS

Rod	Time (s)	Cladding Temperature at 0.580 m (K)	Cladding Temperature at 0.630 m (K)	Cladding Temperature at 0.680 m (K)	Fuel Centerline Temperature at 0.580 m (K)
605-5	12.9	1305	1194	1110	1460
605-6	12.7	1376	1267	1169	1600
605-7	11.2	1316	1202	1113	1471
605-8	11.5	1385	1277	1176	1617

temperature increased ∿400 K at 0.580 m and decreased by ∿10 K at 0.680 m. After CHF at 0.680 m, the predicted temperature increased to within 200 K of the 0.580 m cladding surface temperature.

The peak in cladding surface temperatures at about 11 s followed by a gradual decrease to lower values, as shown in Figures 7-10, was due to the net energy deposition in the cladding. During steady state operation and prior to CHF, the amount of energy transferred to the cladding by the fuel is offset by the amount of energy transferred from the cladding to the coolant by nucleate boiling and forced convection. After CHF, the cladding surface heat transfer coefficient rapidly decreased, and the amount of energy deposited in the cladding exceeded the amount of energy transferred from the cladding to the coolant and flow shroud, and resulted in the rapid cladding temperature increases shown in Figures 7-10. The fuel enthalpy was predicted to decrease due to a decrease in fuel rod power, and the net amount of energy deposition in the cladding subsequently decreased after the peak, while the rate of energy transfer from the cladding to the steam and shroud remained relatively constant. This caused the cladding temperature to decrease and finally level out at a lower temperature.

The cladding surface temperatures at the thermocouple locations were predicted to be higher for the irradiated rods (605-6 and 605-8) than for the corresponding unirradiated rods (605-5 and 605-7), as indicated in Table III and Figures 7-10. Even though cladding creep was predicted to occur in the irradiated rods, a predicted fuel densification of 3% resulted in initially larger fuel-to-cladding gap sizes for the irradiated rods as compared with the unirradiated rods (0.121 mm versus 0.108 mm). The larger gap widths subsequently resulted in about 8% higher initial fuel enthalpies in the irradiated rods. The higher fuel stored energies contributed to the predicted higher cladding surface temperatures (∿70 K at the 0.580 m location) during the transient. In comparison with the LOC-3 test predictions, the unirradiated rod gaps were larger than the predicted irradiated rod gaps and the opposite effect was predicted.

The slight discontinuities in cladding surface temperatures and fuel centerline temperature between 4 s and 10 s, and cladding surface temperatures between 28 s and 31 s (shown in Figures 7 through 10) are insignificant and are not expected to occur during the LOC-5 test. The first discontinuity, shown in Figures 7-10 between 4 s and 10 s, is due to the method of calculation of heat transfer from the fuel to the cladding. FRAP-T5 calculates two fuel-to-cladding gap sizes, thermal and structural. The thermal gap size is used to calculate heat transfer from the fuel to the cladding prior to cladding failure. The structural gap size is used for pellet-cladding mechanical interaction calculations. Prior to cladding failure, the thermal gap size was calculated to be less than the structural gap size. Upon cladding failure, the thermal gap size was set equal to the structural gap size by FRAP-T5, which resulted in a sudden decrease in the calculated gap heat transfer coefficient with a corresponding decrease in cladding surface temperature and slower rate of decrease in the fuel centerline temperature (due to a decrease in fuel surface heat flux). The second discontinuity, shown in Figures 7-10 between 28 s and 31 s, was due to the method used in modifying the RELAP4 thermal-hydraulic data used in FRAP-T5. The time-to-CHF calculated by RELAP4 and was predicted to occur uniformly along the entire length of the rod. The data was then modified to account for the expected axial distribution of time-to-CHF. This modification resulted in the thermal-hydraulic data discontinuity reflected by FRAP-T5 between 28 s and 31 s.

4.1.1.2 Cladding peak temperature response. The predicted location of the peak cladding surface temperature of Rod 605-5 is shown as a function of time in Figure 11. The peak cladding temperature was predicted to move from 0.3 m to 0.07 m and then back into the high power region as CHF propagated upwards from the bottom of the fuel rod. Similar behavior is predicted for the other fuel rods. The shift of the predicted peak cladding temperature at 28 s down to 0.3 m was due to a discontinuity in thermal hydraulic conditions produced by the previously mentioned time-to-CHF modelling, and is not expected to occur in the LOC-5 test.

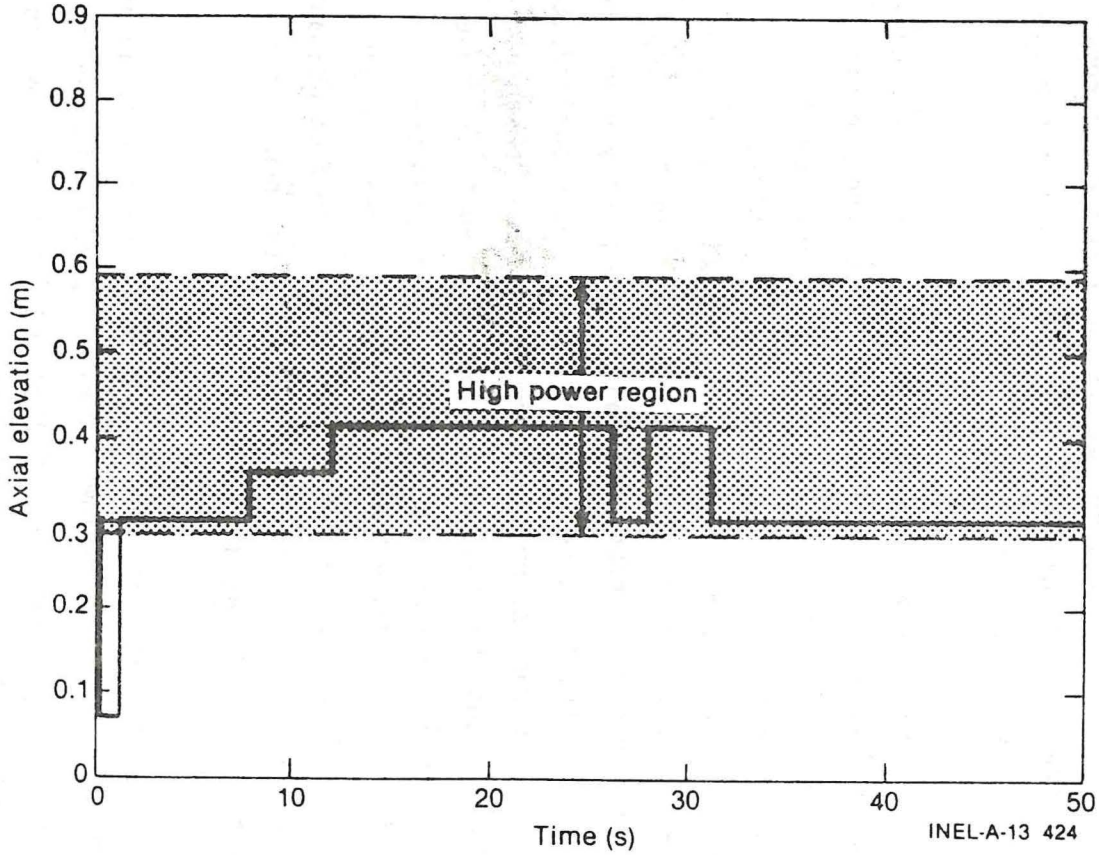

Fig. 11 Rod 605-5 peak cladding temperature location as a function of time.

The predicted cladding surface temperature at the location of cladding failure is shown in Figure 12. The cladding surface temperatures of the four fuel rods are predicted to initially decrease after blowdown due to the onset of nucleate boiling of the coolant as the system depressurizes and the coolant saturates. CHF is predicted to occur at the location of cladding failure (0.30 m for all rods) 0.90 s after blowdown and the cladding temperatures are then predicted to increase rapidly as shown in Figure 12.

The cladding temperatures of the low pressure Rods 605-5 and 605-6, as shown in Figure 12, are predicted to reach the β-phase (>1250 K) prior to rod failure. The cladding was predicted to collapse when the temperatures entered the low-yield-stress $\alpha+\beta$ - phase (1105 to 1245 K) while the system pressure was still higher than the rod internal pressure. The collapse of the cladding resulted in an improved gap conductance and a subsequently higher heat flux from the fuel to the cladding. As the system depressurized, the difference between the rod internal pressure of the low pressure Rods 605-5 and 605-6 and the system pressure continued to decrease until the rod internal pressures exceeded the system pressure, consequently initiating cladding ballooning. The increase in gap width due to the cladding ballooning reduced the gap conductance and corresponding heat flux and the cladding temperatures (now in the β-phase) began to level off and decrease.

The predicted cladding temperature of the low pressure irradiated Rod 605-6 at approximately 5 s is lower than the predicted cladding temperature of the low pressure unirradiated Rod 605-5, as shown in Figure 12. This is due to rod internal pressure differences between Rod 605-5 and Rod 605-6 at the time of blowdown, and the effects of prior irradiation on Rod 605-6. Similar differences in behavior between the high pressure irradiated Rod 605-8 and the high pressure unirradiated Rod 605-7 are also predicted to occur. The effects of prior irradiation will be discussed in the next subsection, since these effects influence the cladding temperatures by influencing the mechanical response of the fuel rods during the blowdown.

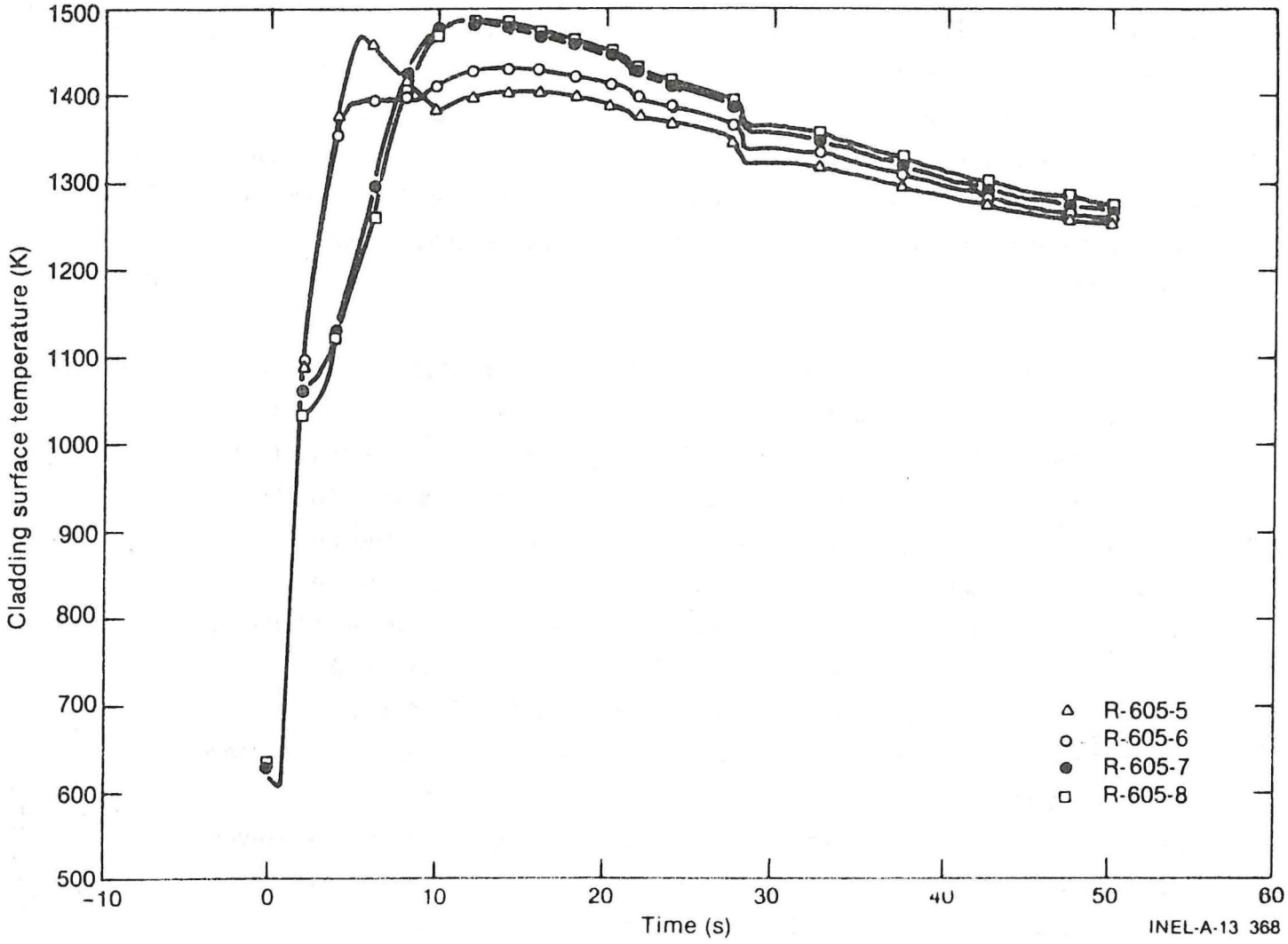

Fig. 12 Cladding temperature at the location of failure as a function of time for the LOC-5 fuel rods.

In Figure 12, the cladding temperatures of the high pressure Rods 605-7 and 605-8 are predicted to increase into the high α range (>1050 K) by 2 s. At a predicted cladding temperature of approximately 1050 K, the rate of temperature increase lessened for both rods indicating that the cladding began to deform outward and subsequently changed the heat flux from the fuel to the cladding. After cladding failure the temperature is predicted to continue increasing until approximately 12 s before leveling off and decreasing to about 1260 at 50.0 s. The increase in cladding temperature after cladding failure was the result of the decreased gap conductance due to early cladding deformation causing a decrease in the fuel surface heat flux, and subsequently a prolonged period of elevated fuel temperature.

The predicted behavior of the cladding temperatures of the low pressure Rods 605-5 and 605-6 differ significantly from the behavior of the high pressure rods, as shown in Figure 12. The cladding of the low pressure rods is predicted to deform slowly, as compared to the cladding of the high pressure rods, and therefore, the cladding temperatures of the low pressure rods are predicted to increase rapidly for a longer period of time, with subsequently higher cladding temperatures at the time of failure. The cladding of the high pressure rods is predicted to deform as soon as the cladding temperatures achieve the high α range. As a consequence, the cladding of the high pressure rods fails at lower temperatures than the cladding of the low pressure rods, as shown in Figure 12, but achieves higher peak cladding temperatures than the low pressure rods due to a greater amount of fuel stored energy after 10 s.

4.1.2 Fuel Rod Mechanical Response. The predicted mechanical response of the LOC-5 fuel rods in the region of cladding failure are discussed in this subsection. The mechanical response at the thermocouple locations will not be discussed because the extent of fuel rod deformation at those locations was found to be insignificant (cladding hoop strains <0.1%).

The differences between the fuel rods in the predicted times to failure, as shown in Table IV, are due to differences in rod internal pressure at the time of blowdown and the prior irradiation history of the rods.

Fuel rod internal pressure as a function of time at the location of predicted cladding failure is shown in Figure 13. The small local pressure peaks between 2 s and 3 s in the low pressure rods (605-5 and 605-6) are due to initial compressive stresses followed by tensile stresses that were predicted for these rods as the cladding surface temperatures entered the high α-phase and cladding deformation occurred. As the system depressurized, the cladding on the low pressure rods initially collapsed then began to deform outwards, and the internal pressures consequently peaked then returned to their precollapse values.

The difference in pressures between the irradiated fuel rods (605-6 and 605-8) and the corresponding unirradiated fuel rods (605-5 and 605-7), as shown in Figure 13, is due to the difference in free gas volume of the irradiated rods as compared to the unirradiated rods (10.1 cm^3 versus 6.8 cm^3). The larger free gas volume in the irradiated rods was due, in part, to an estimated 3% fuel densification in the Saxton reactor. As the irradiated rod fuel temperatures increased, the additional free gas volume was decreased due to fuel pellet expansion. Additionally, the gap sizes of the previously irradiated fuel rods (605-6 and 605-8) were greater than the gap sizes of the counterpart unirradiated fuel rods (605-5 and 605-7) at the beginning of the transient; and hence, higher rod internal pressures due to more extensive fuel expansion and higher gap temperatures occurred.

The high pressure fuel rods (605-7 and 605-8) began to deform as soon as the cladding temperatures reached the high temperature range (>1050 K) 2 s after blowdown. The sudden decrease in rod internal pressure at 4.4 s in Figure 13 was caused by cladding failure and nearly immediate equalization with the system pressure. After rod

TABLE IV

CLADDING YIELD STRESS AT TIME OF ROD FAILURE

Rod	Time of Failure (s)	Cladding Temperature at Location of Failure (k)	Yield Stress at Location of Failure (MPa)
605-5	10.00	1388	13.13
605-6	8.80	1396	14.57
605-7	4.40	1158	20.74
605-8	4.32	1140	27.09

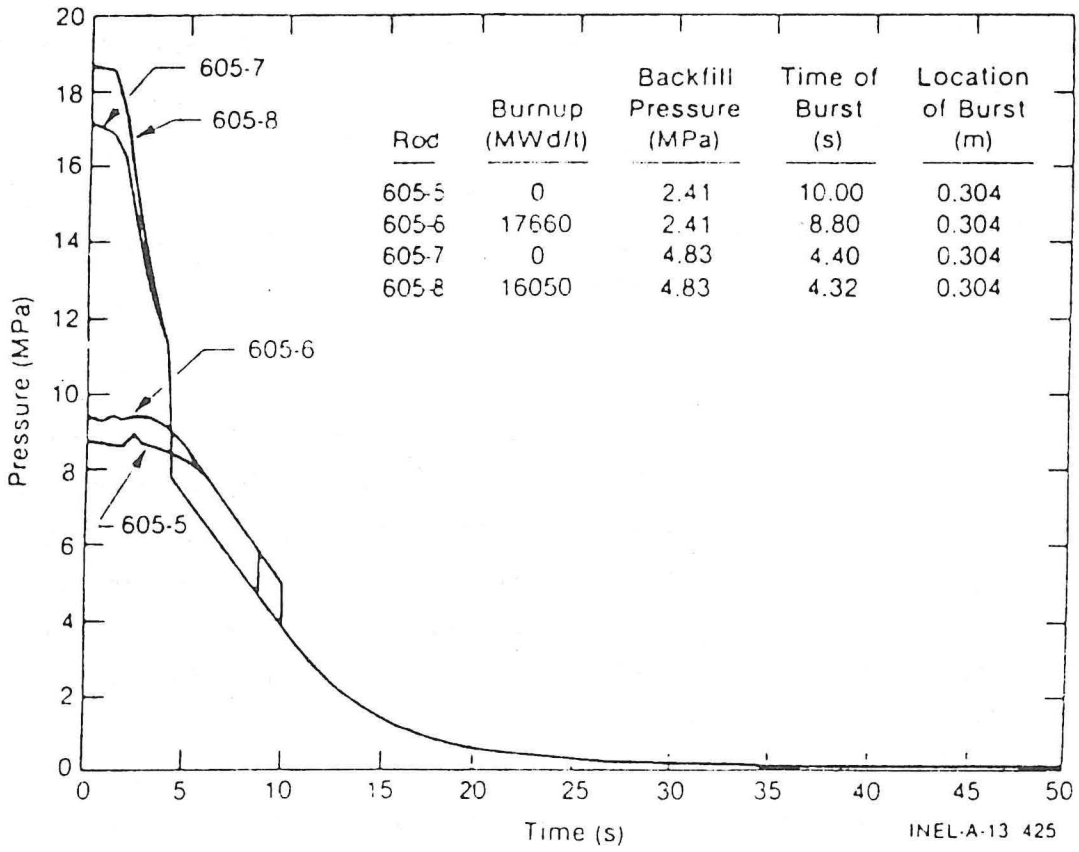

Rod	Burnup (MWd/t)	Backfill Pressure (MPa)	Time of Burst (s)	Location of Burst (m)
605-5	0	2.41	10.00	0.304
605-6	17660	2.41	8.80	0.304
605-7	0	4.83	4.40	0.304
605-8	16050	4.83	4.32	0.304

Fig. 13 Fuel rod internal pressure at the location of cladding failure as a function of time.

failure, the rod internal pressure response follows the depressurization of the system. The steepness of the high pressure Rod 605-7 and 605-8 pressure responses indicates that these fuel rods will deform at nearly the same rate as the system depressurization rate until cladding failure.

The response of the low pressure rods (605-5 and 605-6) is slower than the response of the high pressure rods (605-7 and 605-8) due to the lesser degree of rod internal prepressurization, as shown in Figure 13. The rod internal pressures of the low pressure rods did not begin to decrease until the system pressure decreased sufficiently to allow outward cladding deformation. At $\sim$6 s the pressure response of both low pressure rods is identical and follows system depressurization until their respective times of failure.

The nearly identical pressure responses of the rods with the same prepressurization, as shown in Figure 13, is due to the extent of the predicted annealing of the cladding of the irradiated rods (605-6 and 605-8) prior to cladding failure. FRAP-T5 calculates the extent of cladding annealing as a function of the temperature of the cladding and the time the cladding is at that temperature. The slightly different pressure responses of the rods with the same prepressurization are most noticeable during the first 2 seconds of the blowdown, as shown in Figure 13. After the first 2 s of the blowdown, the predicted responses of the rods with the same prepressurization (605-7 and 605-8) are nearly identical. The predicted pressure responses shown in Figure 13 are consistent with the pressure responses seen in the LOC-3 test.

The high pressure rods (605-7 and 605-8) are predicted to mechanically respond nearly identically in the blowdown, as shown in Figure 14. Cladding deformation was predicted to begin as soon as the cladding temperatures reached the high α phase. The high pressure irradiated Rod 605-8 strained at a slightly faster rate than the high pressure unirradiated Rod 605-7, yet achieved a greater amount of strain at failure (21.8% compared to 15.1%). The high pressure rods

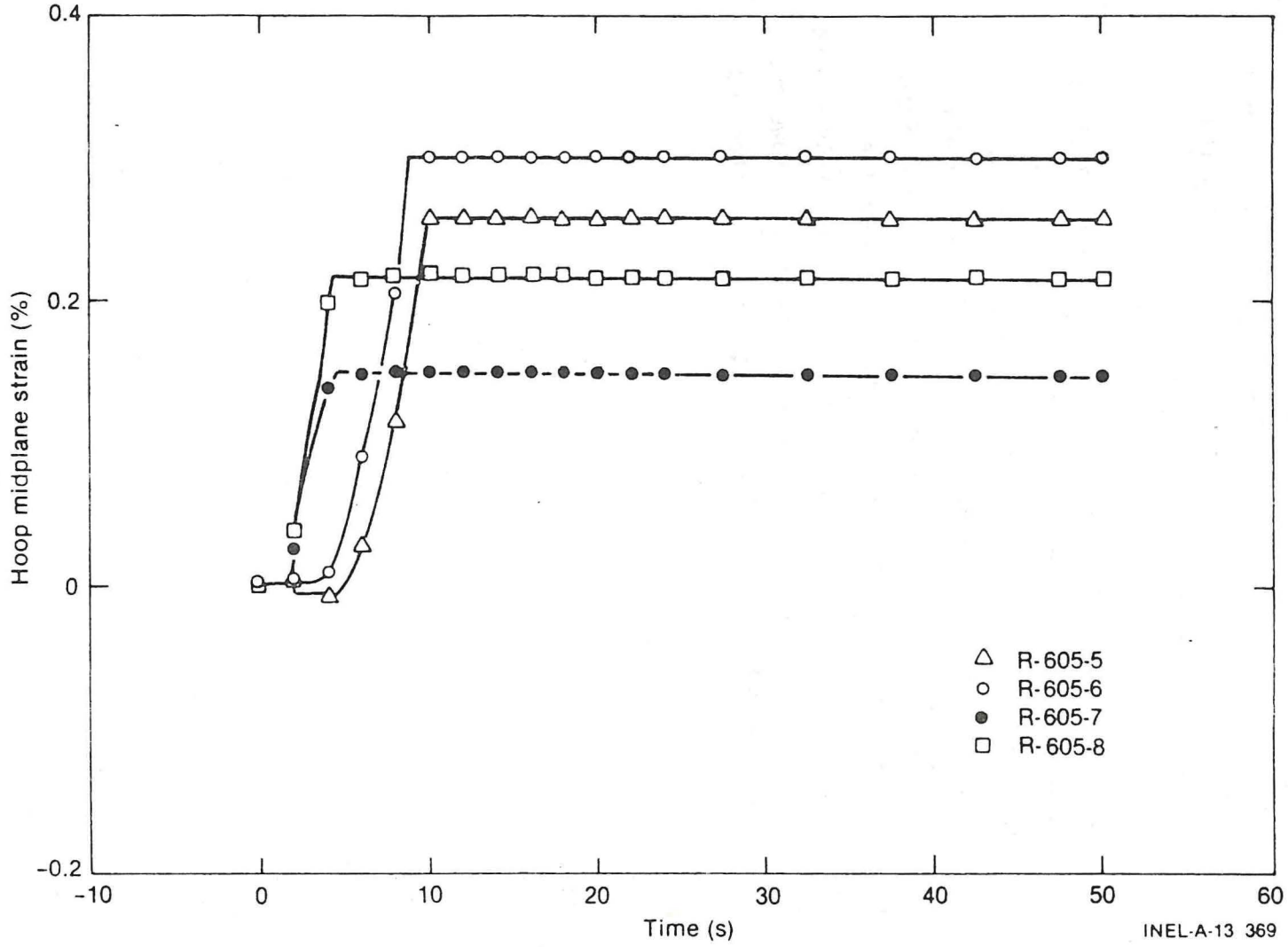

Fig. 14 Hoop midplane strain at the location of cladding failure as a function of time.

failed in the $\alpha + \beta$ phase (1105 K to 1245 K) as the predicted cladding yield stresses decreased. In Table IV, the cladding yield stress of the irradiated Rod 605-8 is higher than the cladding yield stress of the unirradiated Rod 605-7. Hence, the irradiated Rod 605-8 is predicted to strain more prior to cladding failure, than is the unirradiated Rod 605-7. As shown in Figure 15, the length of the ballooned region is predicted to be the same for both rods; however, the amount of outward deformation is greater for the irradiated Rod 605-8 than for the unirradiated Rod 605-7.

The low pressure rods (605-5 and 605-6) failed in the β phase (>1250 K) with strains at failure of 25.99% for Rod 605-5 and 30.21% for Rod 605-6, as shown in Figure 14. The cladding of the low pressure irradiated fuel Rod 605-6 has a higher calculated yield stress than the cladding of the low pressure unirradiated Rod 605-5. Hence, the irradiated rod is predicted to strain more than the unirradiated rod. This is also shown in Figure 15. The length of the ballooned region is predicted to be the same for both rods; however, the amount of outward deformation is greater for the irradiated rod.

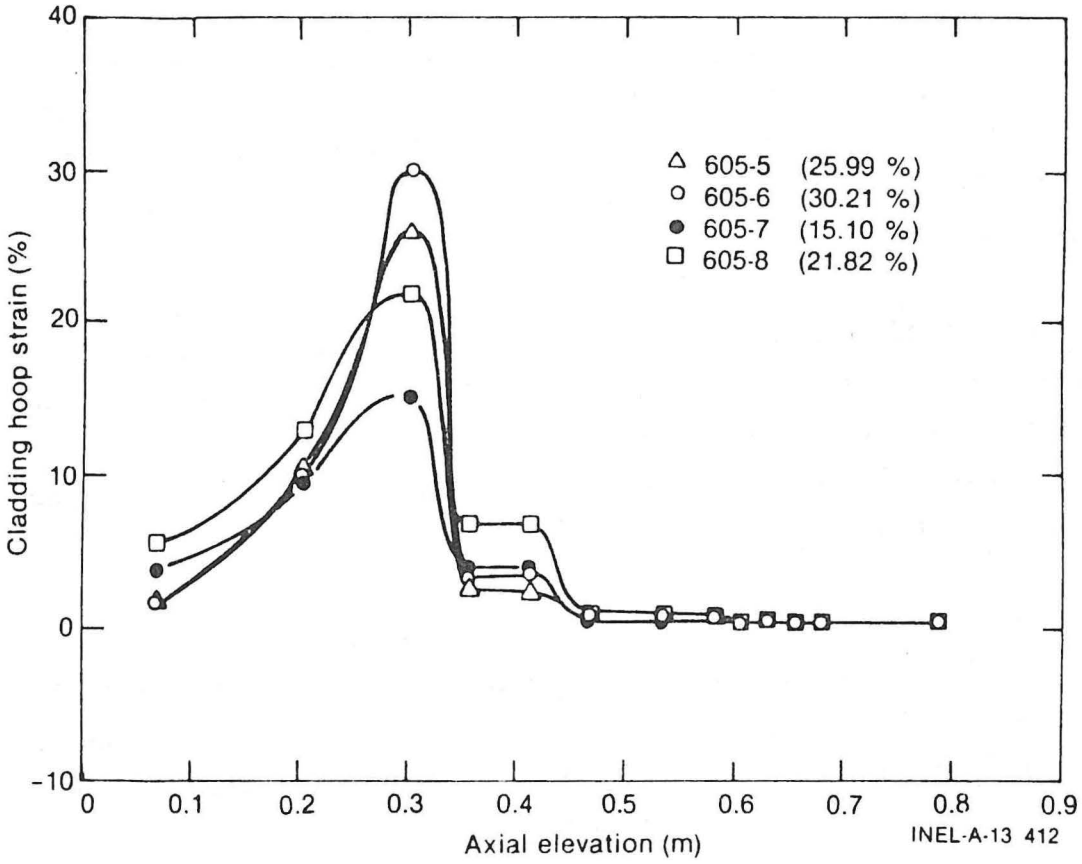

Fig. 15 Axial distribution of cladding hoop strain at the time of cladding failure.

5. CONCLUSIONS

Test LOC-5 is designed to experimentally determine fuel rod behavior during a simulated double-ended cold-leg break LOCA. The separate effects of fuel rod internal pressure and prior irradiation of the four Saxton rods will be investigated during the blowdown transient.

The predicted test rod powers during the initial steady state phase and during the blowdown transient are based on the results of the reactor physics calculations discussed in the Test LOC-3 Experiment Predictions Document. The predicted peak linear rod power is 52.0 kW/m across an axially centered 30 cm region.

The predicted system thermal-hydraulics during the simulated double-ended cold-leg break LOCA are the same as those presented for the Test LOC-3. A modification to the thermal-hydraulic response to account for the axial variation in time-to-CHF was implemented to account for the CHF axial propagation observed in the Test LOC-3.

Rod failure is predicted to occur around 4 s for the higher pressure Rods 605-7 and 605-8, and from 9 to 10 s for the lower pressure Rods 605-5 and 605-6. The cladding temperatures at the time of rod failure are not expected to achieve the β phase for the higher pressure rods but are expected to achieve the β phase for the lower pressure rods.

The strain at failure is expected to be less in the previously unirradiated fuel rods (605-5 and 605-7) than in the previously irradiated fuel rods (605-6 and 605-8) . This is due to the lower yield stresses of the former as compared to the latter at the time of failure. The ability of FRAP-T to accurately predict the amount of annealing in the previously irradiated rods influences the calculation of cladding deformation and cladding temperature. If FRAP-T overpredicts the amount of cladding annealing, the cladding surface temperatures will be likewise overpredicted due to an overprediction of the extent of cladding deformation prior to cladding failure.

The data of Test LOC-5 will be valuable in assessing the models of the analytical codes used to make these predictions. These data combined with the data from all LOCA single-rods tests will be used to characterize fuel rod behavior during a simulated double-ended cold-leg break LOCA.

6. REFERENCES

1. J. M. Broughton and P. E. MacDonald, Light Water Reactor Fuel Behavior Program Description: PBF-LOCA Experiment Requirements, TFBP-TR-201 (January 1975).

2. L. D. Schlenker, Thermal Fuels Behavior Program, Project Description Document, Appendix E, Loss-of-Coolant Accident, TFBP-TR-103 (May 1975).

3. T. R. Yackle, PBF-LOCA Single Rod Tests Program Experiment Requirements Document, TFBP-TR-279 (July 1978).

4. T. R. Yackle, Loss-of-Coolant Accident, Test LOC-5, Experiment Operating Specification, TFBP-TR-309 (August 1979).

5. T. R. Yackle, et al., Loss-of-Coolant Accident Test Series, Test LOC-3, Experiment Predictions, TFBP-TR-314 (April 1979).

6. J. A. Dearien, et al., FRAP-S3 - A Computer Code for the Steady State Analysis of Oxide Fuel Rods, TFBP-TR-164 (October 1977).

7. T. R. Yackle, M. E. Waterman, L. L. McKie, PBF-LOCA Test Series, Test LOC-3, Quick Look Report, TFBP-TR-328 (July 1979).

APPENDIX A

FRAP-T5 CODE INPUT SUMMARY

FRAP-T5[C-1] code inputs are summarized in Tables A-I and A-II. Sample FRAP-T input lists are provided in Table A-III. Specific modeling assumptions for the FRAP analyses are as follows:

(1) Thirteen axial nodes are used to model the test rod. This noding provides a close mockup of test rod thermocouples and regions of interest within the test section.

(2) Coleman Relocation and free thermal expansion with the Ross & Stoute gap conductance correlation, are used to model the pellet-to-cladding heat transfer. Fuel conductivity is corrected for cracking using the FRAP-S3 formula.

(3) Cathcart cladding oxidation model is used, assuming an inital test cladding oxide thickness of 3.01 m and test shroud oxide thickness of 1.40 m. These oxide thicknesses resulted in cladding and shroud emissivities of 0.7 and 0.5, respectively at the beginning of the blowdown transient.

(4) The FRAP-T axial gas flow model is used.

(5) Fuel failure is predicted by FRACAS-I.

(6) No cladding cold work or fast neutron exposure is assumed.

The test fuel radial and axial power profiles are from reactor physics calculations. Assumptions of importance concerning these profiles are:

(1) Constant axial and radial power profiles assumed with time.

TABLE A-I

FRAP CODE INPUT SUMMARY[a]

Fuel Region	Active Length (mm)	889.1
	Material	UO_2
	Enrichment (%)	12.5
	Mean Pellet Height (mm)	15.24
	Mean Pellet Diameter (mm)	8.534[b]/8.439[c]
	Pellet Shoulder Radius (mm) (Dishing Radius)	3.30[b]/4.01[c]
	Dish Depth (mm)	0.343[b]/1.57[c]
	Mean Geometric Density (g/cm^3)	10.36[b]/10.14[c]
	RMS Roughness (m)	2.159
	Cold State Volume of Pellet Dish (mm^3)	11.78[b]/63.53[c]
Cladding Region	Material	zircaloy-4
	Mean Cladding ID (mm)	8.75[b]/8.688[c]
	Mean Cladding OD (mm)	9.93[b]/9.864[c]
	RMS Roughness (m)	1.143
Plenum Region	Fill Gas Composition	100% Helium
	Plenum Volume (cm^3)	2.88
	Cold Gas Pressure (MPa)	Rods 934, 839, p = 2.41 MPa Rods 935, 912, p = 4.83 MPa
	Spring Length (mm)	73.66
	Spring Coil	8.622
	Spring Wire Diameter (mm)	1.02
	Number of Spring Coils	20
Flow Shroud Region	Coolant Flow area (mm^2)	235[b]/239[c]

a nominal dimensions used

b unirradiated fuel rods

c irradiated rods

TABLE A-II

AXIAL POWER PROFILE OF TEST LOC-5

Distance From Bottom of Fuel Stack (m)	Normalized Axial Power[a]
0	0.560
0.032	0.610
0.083	0.770
0.125	0.940
0.183	1.090
0.225	1.165
0.283	1.230*
0.438	1.230*
0.583	1.200
0.683	1.035
0.732	0.900
0.783	0.750
0.833	0.600
0.879	0.540

* Peak-to-average = 1.23

TABLE A-III

FRAP-T5 CODE INPUT

```
        1         2         3         4         5         6         7         8
12345678901234567890123456789012345678901234567890123456789012345678901234567890

    1    1  -13    0    4    1    1         3
    2                        3    1              5
0.00       50.0                    0.2       0.8891    0.00993    294.2611  0.10
  1.036E04   0.00330  3.43E-04  1.524E-02  1.178E-8                        0.00.0
    3.        1773.
    0.5518    0.8891
      1.10      0.01                                                  1.1
0.02       0.0        0.02       25.0       0.05       25.02      0.05       50.0
     1          1  1.0
0.06913   0.20738   0.30403   0.35909   0.41415   0.46921   0.53702   0.58230
0.60630   0.63030   0.65520   0.68010   0.78710
          0    0
0.10       0.0        0.10       25.0       0.50       50.0
0.019618
598.1            0.0   559.8          8.0   458.2          18.0 417.6            38.0
653.2            50.1
  100  100    50    50     0
350.0      3550.0     350.0      2350.0
= LOC-5 BLOWDOWN ANALYSIS OF FRESH FUEL(2.41MPA,BU=000000)
* GENERAL DATA FOR HEAT-1
01010001   9  2  0.0  1.0  150  1.0  150
* GENERAL LOCATION AND MESH INCREMENT
01010200  0    1
* MESH INCREMENT DATA
01010201   1  0.0009388  4  0.004267  1  0.004375  2  0.0049658
* COMPOSITION OVERLAY
0.010301  1   5   3   5   2   8
* SOURCE DISTRIBUTION CARDS
01010401   .8853   1   .8985  2   .9351  3   .9832  4   1.107  5
01010403  0.000    8
* INITAL TEMPERATURE DISTRIBUTION
01010601    590.00    9

     1    16    14
42.189     0.0        38.814     1.0        36.367     1.5        35.354     1.75
34.384     2.0        34.089     2.5        5.617      2.8        9.053      3.0
5.167      5.0        3.268      10.0       2.813      12.0       2.109      20.0
1.994      22.0       1.591      31.0       1.47       40.0       1.428      50.0
     0.560      0.006      0.610      0.038      0.770      0.089      0.940      0.131
     1.090      0.189      1.165      0.231      1.230      0.289      1.230      0.489
     1.200      0.589      1.035      0.689      0.900      0.738      0.750      0.789
     0.600      0.839      0.540      0.883
     4                                7    :    32
1.143      2.155
     1    20              3.686E-6  2.4100E6  .0736632  0.008622  0.00102     294.26
1.0
    13
     1    2    3    4    5    6    7    8    9   10   11   12   13
0.00       50.        10.          TIME(S),LOC-5, 2,41 MPA, BU=0
      500.      2000.        15.      CLAD SURFACE TEMPERATURE (K)

        1         2         3         4         5         6         7         8
12345678901234567890123456789012345678901234567890123456789012345678901234567890
```

```
         1         2         3         4         5         6         7         8
12345678901234567890123456789012345678901234567890123456789012345678901234567890

    1    1  -13    0    4    1    1          3
                                  3          1                    5
0.00       50.0                                0.8891     .009842    294.2611   0.10
10576.46   0.004009       1.57E-3 1.524E-02  6.353E-8                1.525824E6    0.0
    2.       1773.
      1.10       0.01                                                    1.1
0.02       0.0        0.02       25.0       0.05       25.02      0.05       50.0
    1          1  1.0
0.06913    0.20738    0.30463    0.35909    0.41415    0.46921    0.53702    0.58230
0.60630    0.63030    0.65520    0.68010    0.78710
         0    0
0.05       0.0        0.10       20.0       0.50       50.0
0.019719
598.1           0.0  559.8           8.0  458.2           18.0 417.6           38.0
653.2           50.1
  100  100    50    50    0
350.0      3550.0     350.0      2350.0
* LOC-5 BLOWDOWN ANALYSIS OF SAXTON ROD(2.41MPA, BU=17660.MWD/TU)
* GENERAL DATA FOR HEAT-1
01010001   9  2  0.0  1  .00  1.0  400
* GENERAL LOCATION AND MESH INCREMENT
01010200  0   1
* MESH INCREMENT DATA
01010201              5 0.0042195  1 0.004341  2 0.004931
* COMPOSITION OVERLAY
01010301 1  5  3  6  2  8
* SOURCE DISTRIBUTION CARDS
01010401  .8840  1   8918  2  .9228  3  .9711  4  1.095  5
01010402  0.000   8
* INITAL TEMPERATURE DISTRIBUTION
01010601   590.00   9

    1   16   14
42.189     0.0        38.814     1.0        36.367     1.5        35.354     1.75
34.384     2.0        34.069     2.5        9.617      2.8        9.053      3.0
6.167      5.0        3.266      10.0       2.813      12.0       2.109      20.0
1.994      22.0       1.591      31.0       1.47       40.0       1.428      50.0
     0.560      0.006      0.610      0.038      0.770      0.069      0.940      0.131
     1.090      0.189      0.165      0.231      1.230      0.289      1.230      0.489
     1.200      0.589      0.035      0.689      0.900      0.738      0.750      0.789
     0.600      0.839      0.540      0.883
    4                                 7    1   32
1.143      2.159
    1   20             3.836E-6  2.4100E6   .0736632  0.008622   0.00102      294.26
1.0
   13
    1    2    3    4    5    6    7    8    9   10   11   12   13
0.00       50.        10.        TIME(S),LOC-5, 2.41 MPA, BU=14910MWD/TU
     500.       2000.       15.       CLAD SURFACE TEMPERATURE (K)
     500.       4000.        7.       FUEL CENTERLINE TEMPERATURE (K)

         1         2         3         4         5         6         7         8
12345678901234567890123456789012345678901234567890123456789012345678901234567890
```

(2) Neutron transport into the test section has no axial dependency.

(3) ANS 5.1 standard on decay fission product heating is assumed.

(4) The figure-of-merit for the depleted test fuel is assumed equal to the fresh fuel.

(7) Test section blowdown occurs at time 0. The first of two planned transient test section power reductions occurs at minus 0.4 s, the second at 8 to 10 s.

(8) The LOC-5 test rod-shroud geometry, percent theoretical density, and surface roughnesses are as noted in the LOC-3 ESD (TFBP-TR-259).

(9) The FRAP-T convective heat transfer coefficients were calculated by RELAP and input via tape. Radiation heat transfer is calculated by FRAP-T as follows:

$$q_{rad} = F_{cs} \left(T_{cladding}^4 - T_{shroud}^4 \right)$$

$$h_{rad} = q_{rad} \left(T_{cladding} - T_{bulk} \right)$$

where $F_{cs} = E_{cladding} + \frac{D_{cladding}}{D_{shroud}} \left(F_{shroud}^{-1} - 1 \right)^{-1}$

E = Emissivity

(10) FRAP-S was used to assess the effects of burnup on the Saxton derived test fuel. The effects of densification fuel swelling, and cladding creep were incorporated in the FRAP-T analyses.